Queensland University of Technology
Brisbane Australia

This may be the author's version of a work that was submitted/accepted for publication in the following source:

Liu, Qian, Kumagai, Shohei, Manzhos, Sergei, Chen, Yingqian, Angunawela, Indunil, Nahid, Masrur Morshed, Feron, Krishna, Bottle, Steven E., Bell, John, Ade, Harald, Takeya, Jun, & Sonar, Prashant
(2020)
Synergistic use of pyridine and selenophene in a diketopyrrolopyrrole-based conjugated polymer enhances the electron mobility in organic transistors.
Advanced Functional Materials, *30*(34), Article number: 2000489.

This file was downloaded from: https://eprints.qut.edu.au/205494/

© 2020 WILEY-VCH Verlag GmbH and Co. KGaA, Weinheim

This work is covered by copyright. Unless the document is being made available under a Creative Commons Licence, you must assume that re-use is limited to personal use and that permission from the copyright owner must be obtained for all other uses. If the document is available under a Creative Commons License (or other specified license) then refer to the Licence for details of permitted re-use. It is a condition of access that users recognise and abide by the legal requirements associated with these rights. If you believe that this work infringes copyright please provide details by email to qut.copyright@qut.edu.au

License: Creative Commons: Attribution-Noncommercial 4.0

Notice: *Please note that this document may not be the Version of Record (i.e. published version) of the work. Author manuscript versions (as Submitted for peer review or as Accepted for publication after peer review) can be identified by an absence of publisher branding and/or typeset appearance. If there is any doubt, please refer to the published source.*

https://doi.org/10.1002/adfm.202000489

Liu, Qian, Kumagai, Shohei, Manzhos, Sergei, Chen, Yingqian, Angunawela, Indunil, Nahid, Masrur Morshed, Feron, Krishna, Bottle, Steven E., Bell, John, Ade, Harald, Takeya, Jun, & Sonar, Prashant (2020) Synergistic use of pyridine and selenophene in a diketopyrrolopyrrole-based conjugated polymer enhances the electron mobility in organic transistors. Advanced Functional Materials, 30(34), Article number: 2000489.

Abstract

To achieve semiconducting materials with high electron mobility in organic field-effect transistors (OFETs), low-lying energy levels (highest occupied molecular orbital <HOMO> and lowest unoccupied molecular orbital <LUMO>) and favourable molecular packing and ordering are two crucial factors. In this work, we report that the incorporation of pyridine and selenophene into the backbone of a diketopyrrolopyrrole (DPP)-based copolymer produces a high-electron-mobility semiconductor, PDPPy-Se. Compared with analogous polymers based on other DPP derivatives and selenophene, PDPPy-Se features a lower LUMO that could decrease the electron transfer barrier for more effective electron injection, and simultaneously a lower HOMO that, however, could increase the hole transfer barrier to suppress the hole injection. Combined with thermal annealing at 240°C for thin film morphology optimization to achieve large-scale crystallite domains with tight molecular packing for effective charges transport along the conducting channel, OFET devices fabricated with PDPPy-Se behave an *n*-type-dominant performance with an electron mobility (μ_e) as high as 2.22 $cm^2 V^{-1} s^{-1}$ and a hole/electron mobility ratio (μ_h/μ_e) of 0.045. Overall, this study demonstrates a simple yet effective approach to boost the electron mobility in organic transistors by synergistic use of pyridine and selenophene in the backbone of a DPP-based copolymer.

Introduction

Organic semiconducting materials, due to the ease of structural modification, solution processability and low cost compared with their inorganic analogues,[1] have been attracting increased attention especially for the fabrication of flexible, light-weight, and large-scale electronic devices.[2-3] Among reported high-performance polymers, diketopyrrolopyrrole (DPP) has proven one of the most successful building blocks to construct semiconductors for applications in a wide range of electronic devices.[4-20] In the community of organic field-effect transistors (OFETs), the semiconductors are classified as *p*-type, *n*-type and ambipolar materials according to the polarity of the dominant charge carriers flowing along the conducting channel.[6] DPP-based polymers have made significant contributions to the advancement of all types of semiconducting materials. For example, some solution-processible *p*-type polymers based on DPP have been reported to achieve hole mobilities of over 10 $cm^2\ V^{-1}\ s^{-1}$ that are even superior to those of amorphous silicon-based transistors which generally deliver a typical mobility range of 0.1-1.0 $cm^2\ V^{-1}\ s^{-1}$.[21-24] Unlike the high mobility of *p*-type DPP-based polymers in OFETs, it is still challenging to obtain high electron mobility. The lack of strong electron-deficient monomers is one of the reasons, since DPP behaves as an electron acceptor which is easy to copolymerize with various donor groups to obtain a series of new materials that improve the hole mobility. To improve the electron mobility, significant efforts have been devoted to either enhance the electron affinity of DPP moiety or copolymerize with new acceptors. By applying this strategy, some materials have shown excellent electron mobility of over 1.0 $cm^2\ V^{-1}\ s^{-1}$ while maintaining good hole mobility, allowing these materials to be used as ambipolar semiconductors.[25-30] As a caveat to this, the synthesis of DPP starts from aromatic cyano precursors. Thus, the DPP core is always flanked with two aromatic groups. Incorporating flanking groups with strong electron deficiency

into the DPP core is a significant challenge, which is one of the reasons for the difficulty in obtaining *n*-type-dominant DPP-based semiconductors.

Among various reported heterocycle flanked DPP monomers, pyridine flanked DPP (DPPy) has shown its potential in developing high-electron-mobility materials.[25] Although pyridine is not a very strong electron-withdrawing group, the introduction of a nitrogen atom makes it more electron-deficient than all other reported flanking groups like thiophene, furan, selenophene, benzene, naphthalene, benzothiophene and thiozole, making DPPy a stronger acceptor.[31-32] Furthermore, the nitrogen atom in the *ortho* position helps to decrease the steric hindrance with the alkyl groups on DPP unit, resulting in an improved coplanarity. It has been reported that the optimization of polymer backbone coplanarity could strongly enhance the charges (holes and/or electrons) transport in OFETs.[33-34] Several copolymers based on DPPy have demonstrated ambipolar or unipolar *n*-type property with electron mobilities of >1.0 cm^2 V^{-1} s^{-1}.[25, 35-37] Although it is not the only decisive factor, a low-lying LUMO energy level can decrease the electron transfer barrier to facilitate the electron injection from the electrode into the LUMO of the semiconductor. A donor-acceptor (D-A) type backbone structure has been demonstrated to be the most effective method to realize energy level modulation. Because of these factors, we are interested in the selenophene (Se) which is more electron-rich compared with the furan and thiophene analogues, which helps to get low LUMO energy level.[38] Additionally, Se-based materials adopt a more quinoidal structure and thus it possesses a less twisted backbone, leading to a longer and more effective conjugation length.[39-40] Finally, the high polarizability of Se, thanks to its low electronegativity, results in a strong intermolecular Se-Se or Se-aromatic interactions in any Se-based structure, which are also known to be beneficial for charge transport.[39, 41-42]

In this work, we designed and successfully synthesized the copolymer, PDPPy-Se, consisting of DPPy and Se monomers and comprehensively studied this new material's thermal, optical and electronic properties. We report that the incorporation of pyridine and selenophene into the backbone of a DPP-based copolymer simultaneously lowered the HOMO and LUMO energy levels, leading to an increased hole injection barrier and a decreased electron injection barrier, respectively. This is a favourable feature for developing *n*-type-dominant semiconductors. Thus, OFET devices were fabricated with PDPPy-Se films annealed at different temperatures (100, 150, 200, 240°C) to thoroughly evaluate its electrical properties. The polymer film annealed at 240°C is observed to form a more ordered and longer-range crystallite domains with tight molecular packing, which is beneficial for charges transport inside the transistor channel. Combined with the favourable energy levels for electrons injection from electrodes into the polymer in the conducting channel, the transistors exhibited an *n*-type-dominant property with a maximum electron mobility of 2.22 cm^2 V^{-1} s^{-1} and a μ_h/μ_e ratio of 0.045. This study demonstrates that the DPP-based copolymer, PDPPy-Se, bearing pyridine and selenophene groups in the backbone is a promising semiconductor for *n*-type-dominant OFET devices because of its suitable energy levels for easy electrons injection and favourable molecular packing and ordering for effective charge transport in the transistor channel.

Results and Discussion

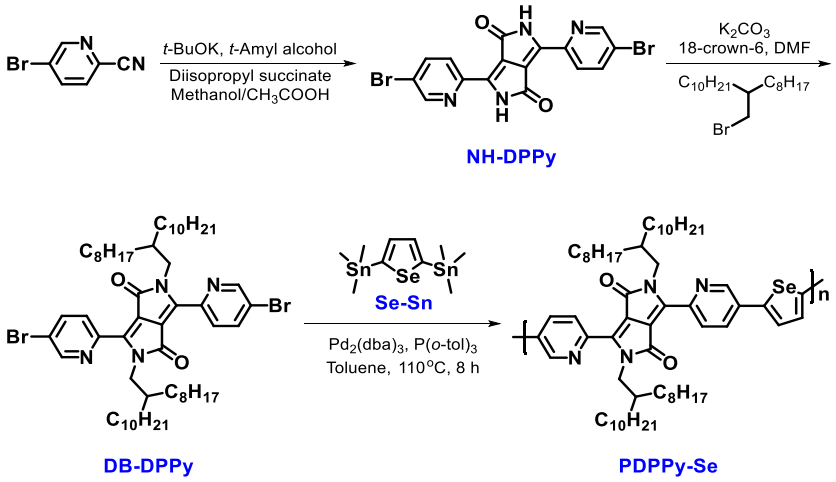

Scheme 1. The synthetic route to the polymer PDPPy-Se.

The synthetic route to the target polymer, PDPPy-Se, is shown in **Scheme 1**. Starting from 5-bromopicolinonitrile, the pyridine flanked DPP core with bromines, 3,6-bis(5-bromopyridin-2-yl)-2,5-dihydropyrrolo[3,4-c]pyrrole-1,4-dione (NH-DPPy), was prepared in one step. Then, the alkylation of compound NH-DPPy was carried out using 2-octyldodecyl bromide in the presence of potassium carbonate (K_2CO_3), 18-crown-6 and dimethylformamide (DMF) at 120°C for 20 hours, giving the monomer, 3,6-bis(5-bromopyridin-2-yl)-2,5-bis(2-octyldodecyl)-2,5-dihydropyrrolo[3,4-c]pyrrole-1,4-dione (DB-DPPy). The synthesis outlined in Scheme followed a modified version of previously reported procedures that produce related materials.[43] The structures of DB-DPPy and commercially available Se-Sn were confirmed by both ^{1}H and ^{13}C NMR spectra. The polymer was ultimately synthesized through Stille coupling polymerization catalysed with tris(dibenzylideneacetone)dipalladium(0) and tri(*o*-tolyl)phosphine [$Pd_2(dba)_3$ and $P(o\text{-tol})_3$] in toluene at 110°C for 8 hours under protection of argon. The purification of PDPPy-Se was carried out by Soxhlet extraction with methanol, acetone, and hexane to remove the remaining catalysts, possible impurities and low-molecular-weight oligomers. The residue was finally

extracted with chloroform to get the pure PDPPy-Se. The polymer has quite a good solubility in chloroform at room temperature with a concentration of >5 mg mL^{-1}. The molecular weight was measured by GPC (gel permeation chromatography) with THF (tetrahydrofuran) as the eluent and polystyrene (PS) as the internal standard. It was determined that the M_n (number-average molecular weight) and M_w (weight-average molecular weight) are 409.1 and 955.4 kDa, respectively, with a PDI (polydispersity index) of 2.34.

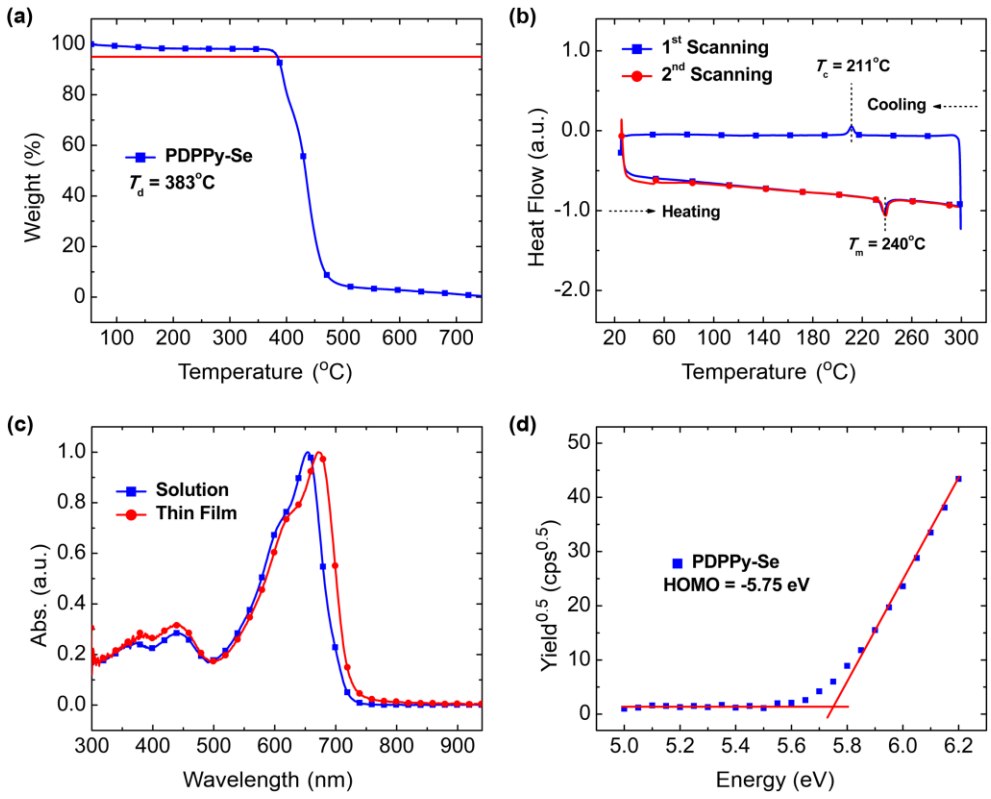

Figure 1. (a) TGA and (b) DSC thermograms of PDPPy-Se; (c) UV-vis absorption spectra of PDPPy-Se in dilute chloroform solution and thin film; (d) PESA measurement.

As shown in **Figure 1a-b**, the thermal behaviour of PDPPy-Se was investigated through thermogravimetric (TGA) and differential scanning calorimetry (DSC) analysis. From the TGA

thermogram, PDPPy-Se shows an excellent thermal stability in nitrogen atmosphere with the decomposition temperature (T_d, 5% weight loss) of 383°C that is high enough for possible practical applications in organic electronics and provides sufficient room for thermal annealing optimization during device characterization. The DSC analysis indicated that a melting transition at ~240°C and a crystalline peak at ~211°C are observed during heating and cooling processes, respectively. This indicated a certain degree of flexibility for the polymer main chain and good crystallinity.[44-45] This feature allows morphology improvement of polymer thin films to form longer-range ordered crystalline domains upon thermal treatment, which will facilitate the charge carrier transport.[46]

The UV-vis absorption spectra in **Figure 1c** showed a usual dual-band feature where the weak absorption band located at 300-500 nm is ascribed to the delocalized π-π* transition and the intense absorption band at 500-750 nm is correlated with the intramolecular charge transfer effects that occurs between pyridine DPP unit and the relatively electron-rich selenophene group. The observable shoulder peak at around 620 nm indicates the distinctive aggregation of polymer chains in both solution and thin film that demonstrates a planar backbone structure and strong intermolecular interactions. The small dihedral angles between pyridine and DPP could contribute to the planarity and the Se···Se interactions due to Se's large atomic radius brought the polymer chains closer even in solution.[25, 40] Specific work upon improved polymer backbone coplanarity for better charge transport in OFETs has been reported.[33-34] From the solution to thin film, the red shift of absorption spectra with the maximum peaks at 654 and 672 nm, respectively, indicated the formation of an ordered polymer mainchain in solid state due to π-π stacking. The onset absorption wavelength in thin film is estimated to be 722 nm which corresponds to the optical bandgap of 1.72 eV.

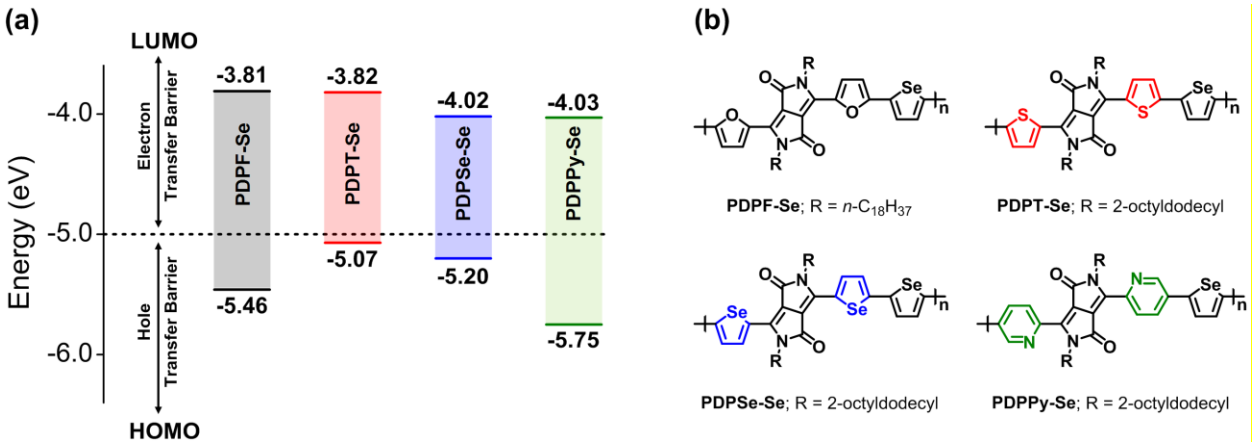

Figure 2. (a) Energy level diagram of four DPP-based polymers and (b) their chemical structures. The energy level values of PDPPF-Se, PDPPT-Se, PDPPSe-Se were extracted from relative publications.[38, 47-48]

To determine the energy levels of PDPPy-Se, a photoelectron spectroscopy in air (PESA) measurement was performed. The polymer was dissolved in chloroform and spin coated on glass substrate for PESA measurements. The onset value was calculated from drawing a tangent to the baseline as shown in **Figure 1d**. The HOMO energy level is found to be -5.75 eV. By incorporation to the optical bandgap, the LUMO energy level is calculated to be -4.03 eV. The comparison of energy level values with those of PDPF-Se, PDPT-Se, and PDPSe-Se as shown in **Figure 2** indicated that both the HOMO and LUMO of PDPPy-Se are decreased. The gaps between LUMO or HOMO and the work function of the electrode (-5.0 eV for Au generally) are defined as the barrier for electrons or holes injection, respectively. Decreased LUMO and HOMO of PDPPy-Se could facilitate the electron injection and simultaneously suppress the hole injection from the electrode into the semiconductor, providing the possibility to obtain high-electron-mobility transistors. This can be partially confirmed by the device characterization results obtained with

PDPT-Se and PDPSe-Se. PDPT-Se has a closest HOMO with gold, delivering a hole mobility of 1.36 $cm^2 V^{-1} s^{-1}$.[48] The lower HOMO of PDPSe-Se makes the corresponding transistor exhibit a relatively low hole mobility of 0.1 $cm^2 V^{-1} s^{-1}$.[38] Although PDPT-Se and PDPSe-Se have different LUMO values, the electron mobility of transistors with both materials is almost the same of 0.1 $cm^2 V^{-1} s^{-1}$. That is also reasonable because another crucial factor to determine the overall performance is the charge transport inside the transistor channel that is strongly influenced by the molecular packing and ordering on substrate. The X-ray diffraction (XRD) patterns indicate that PDPT-Se film displays more ordered crystallite domains with distinct diffraction peaks up to (005) compared with that of PDPSe-Se.[48] Considering the decreased LUMO and HOMO energy levels of PDPPy-Se, combined with thin film morphology optimization, transistors with high electron mobility are expected.

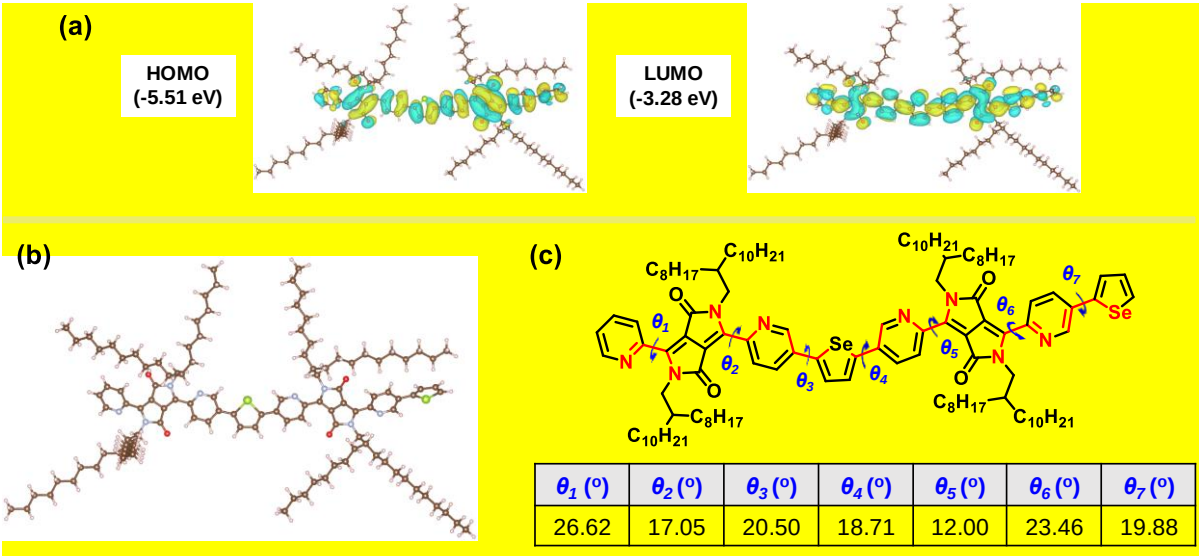

θ_1 (°)	θ_2 (°)	θ_3 (°)	θ_4 (°)	θ_5 (°)	θ_6 (°)	θ_7 (°)
26.62	17.05	20.50	18.71	12.00	23.46	19.88

Figure 3. DFT calculations for polymer dimer with full side chians. (a) HOMO & LUMO molecular orbital distributions; (b) optimized front-view backbone geometry; (c) the optimal dihedral angles between adjacent aromatic units.

DFT (Density Functional Theory) calculations (see Supporting Information for details) were performed on the PDPPy-Se dimer to evaluate the molecular orbitals distribution and the backbone geometry as well as optical properties. As shown in **Figure 3a**, both the HOMO and the LUMO are distributed along the entire polymer dimer backbone, resulting in a relatively minor charge transfer character of the visible transition and its high intensity. The HOMO is localized slightly more on the DPP core than the LUMO. The distribution of the LUMO is helpful for overlapping of molecular orbitals of neighbouring molecules which is beneficial for electron transport in OFETs.[33, 49] The calculated HOMO (-5.51 eV), LUMO (-3.28 eV) and the gap (2.23 eV) are higher than those of the experimental results. The higher LUMO and gap are rational because the onset of thin film absorption spectrum from which the experimental values are estimated is influenced by the vibrational broadening while the DFT calculation is conducted at a fixed equilibrium geometry.[50] The difference of 0.24 eV between the computed and experimentally estimated HOMO is explained by the DFT approximations used as well as uncertainties in PESA. The computed absorption spectrum (**Figure S1**) shows an intense visible peak at 640 nm, in excellent agreement with experiment. **Figure 3b** shows the optimized backbone geometry where we kept the full long branched side chains to, at the maximum extent, reflect the real backbone structure. Visibly the backbone coplanarity is high and the calculated dihedral angles between adjacent aromatic groups are labelled on the chemical structure of polymer dimer in **Figure 3c**. All the dihedral angle values are demonstrated to be less than 30 degrees and support the planar backbone structure of polymer PDPPy-Se, which is expected to play significant roles in crystalline orientation and morphology optimization of polymer films.

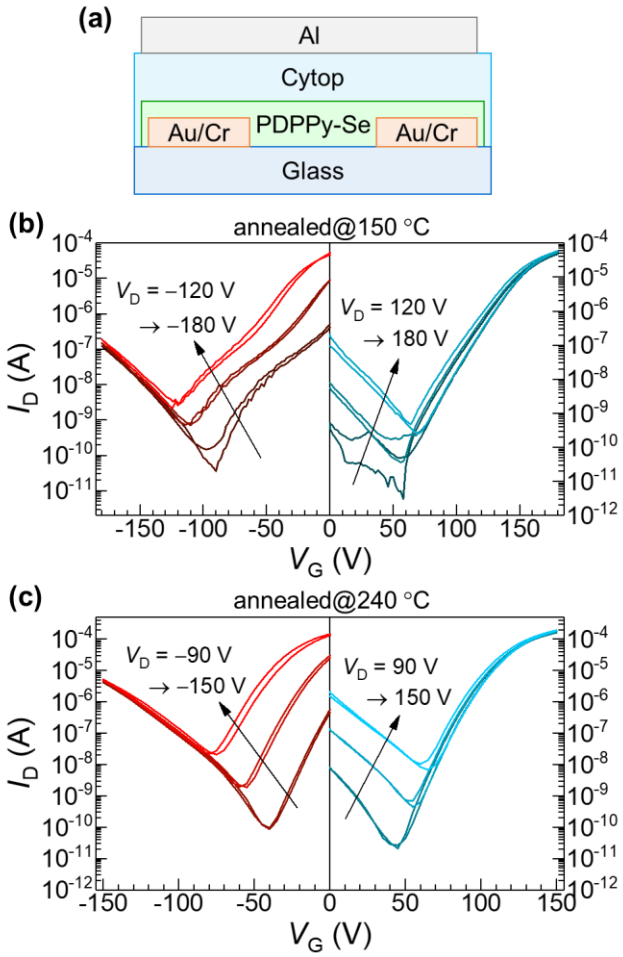

Figure 4. (a) TG/BC OFET structure; Transfer characteristics of an OFET based on PDPPy-Se annealed (b) at 150°C and (c) at 240°C, respectively.

In order to elucidate the charge-transport property of PDPPy-Se, polymer thin film transistors were fabricated. The device schematic with the geometry of top-gate bottom-contact (TG/BC) is shown in **Figure 4a**. On glass substrate with Au/Cr electrodes treated with UV-O_3, 5 mg mL^{-1} chloroform solution of PDPPy-Se was spin-coated and treated with acetonitrile at 100°C on a hotplate for removing water residues by azeotropic effect,[51] followed by thermal annealing at a selected temperature (T_{anneal}) of 100°C, 150°C, 200°C or 240°C in the glovebox. 0.86-1.0 μm-thick Cytop was used as the gate dielectric layer. The detailed fabrication procedure, the output & transfer

curves at different temperatures, and the photograph of a real fabricated device are shown in Supporting Information (**Figure S2**). **Figure 4b** and **4c** display the representative transfer characteristics with T_{anneal} = 150°C and 240°C, respectively. Independent of T_{anneal}, the OFETs based on PDPPy-Se in this study exhibit an *n*-type-dominant ambipolar behaviour as summarized in **Table 1**. This agrees well with the discussion above upon energy levels that simultaneously lowered HOMO and LUMO can supress the holes injection and facilitate the electrons injection, respectively, from the electrodes into the semiconductor. Specifically, annealed, before melting transition temperature (240°C), at 100, 150, and 200°C, the electron mobility and hole mobility exhibit an opposite trend. The electron mobility was first increased from 0.69 $cm^2 V^{-1} s^{-1}$ to 1.10 $cm^2 V^{-1} s^{-1}$ and then decreased to 0.56 $cm^2 V^{-1} s^{-1}$, while the hole mobility was first decreased from 9.0×10^{-2} $cm^2 V^{-1} s^{-1}$ to 1.1×10^{-2} $cm^2 V^{-1} s^{-1}$ and then increased to 2.3×10^{-2} $cm^2 V^{-1} s^{-1}$. After annealing at 240°C (melting transition temperature), both the electron and hole mobility reach a highest value of 2.22 and 1.0×10^{-1} $cm^2 V^{-1} s^{-1}$, respectively. The differences in electron and hole mobilities are ascribed to the annealing-induced variations in film morphology and molecular packing and ordering, which have strong influences on the charges transport in the transistor channel. This will be further discussed below in the atomic force microscopy (AFM) and grazing incidence wide angle X-ray scattering (GIWAXS) sections.

Additionally, this result further confirmed the potential of pyridine DPP as a promising building block to construct high-electron-mobility semiconductors. The structures of reported pyridine DPP-based materials used in OFETs and their device performance are shown in **Scheme S2** and **Table S1**. In **Table 2**, we compiled the data for those materials exhibiting an electron mobility of >1.0 $cm^2 V^{-1} s^{-1}$. The performance of our polymer, PDPPy-Se, with the electron mobility of 2.22

$cm^2\ V^{-1}\ s^{-1}$, is among the best values. It was also observed that pyridine DPP-based materials show either ambipolar or unipolar *n*-type transistor behaviour besides *p*-PDBPy because of its very high LUMO. The ability of pyridine DPP in lowering both the HOMO and LUMO energy levels made significant contributions to facilitate the electron injection compared with other DPP derivatives-based materials.[4] The overall mobility of transistors is determined not only by the energy levels but also closely linked to the film morphology and crystallite orientations. It is also obvious in **Table 2** that an electron mobility of >1.0 $cm^2\ V^{-1}\ s^{-1}$ can be achieved for those materials with LUMO energy levels ranging from -3.47 to -4.33 eV. Therefore, we performed atomic force microscopy (AFM) and 2D-GIWAXS to evaluate the difference in surface morphology and molecular packing and ordering with/without annealing.

Table 1. Performances of OFETs based on PDPPy-Se and comparison with PDPSe-Se.

T_{anneal} [°C]	$\mu_{e,\ max.}$ [a] [$cm^2\ V^{-1}\ s^{-1}$]	$\mu_{e,\ avg.}$ [b] [$cm^2\ V^{-1}\ s^{-1}$]	$\mu_{h,\ max.}$ [a] [$cm^2\ V^{-1}\ s^{-1}$]	$\mu_{h,\ avg.}$ [b] [$cm^2\ V^{-1}\ s^{-1}$]
100	0.69	0.46±0.17	9.0×10^{-2}	$6.1\pm2.8\times10^{-2}$
150	1.10	0.74±0.27	1.1×10^{-2}	$0.4\pm0.4\times10^{-2}$
200	0.56	0.35±0.22	2.3×10^{-2}	$1.1\pm1.0\times10^{-2}$
240 [c]	2.22	1.92±0.30	1.0×10^{-1}	$5.6\pm4.4\times10^{-2}$
200 [d]	0.10	0.10±0.01	1.0×10^{-1}	0.1±0.008

[a] The maximum values with V_D = 180/-180 V (C_i = 1.9 nF cm^{-2}); [b] The average values from 2-3 devices; [c] V_D = 150/-150 V (C_i = 2.2 nF cm^{-2}). [d] The OFET performance of PDPSe-Se (see **Figure 2** for the chemical structure) with a bottom gate bottom contact device configuration; the data are extracted from the reference.[38]

Table 2. Summary of pyridine DPP-based semiconductors and their OFET performance.

Material	HOMO/LUMO	Geometry	T_{anneal}	$\mu_{h,\ max.}/\mu_{e,\ max.}$	Source
PDPPy-Se	**-5.75/-4.03 eV**	**TG/BC**	**150°C**	**1.1×10^{-2}/1.10**	**This work**
PDPPy-Se	**-5.75/-4.03 eV**	**TG/BC**	**240°C**	**1.0×10^{-1}/2.22**	**This work**
PDBPyBT	-5.69/-4.33 eV	TG/BC	100°C	2.78/6.30	Ref. [25]
PPyDPP1-BT	-5.65/-3.47 eV	TG/BC	100°C	0.86/1.05	Ref. [35]
PPyDPP1-4FBT	-5.93/-3.65 eV	TG/BC	200°C	---/1.02	Ref. [35]
PPyDPP2-4FBT	-5.96/-3.69 eV	TG/BC	200°C	---/2.45	Ref. [35]

PDPH	-5.61/-3.93 eV	TG/BC	---	---/1.34	Ref. [37]
PDPF	-5.82/-4.11 eV	TG/BC	---	---/1.19	Ref. [37]
PPyDPP1-4FTVT	-5.86/-3.66 eV	TG/BC	200°C	---/1.19	Ref. [35]
PPyDPP2-4FTVT	-5.89/-3.67 eV	TG/BC	200°C	---/1.35	Ref. [35]
PDBPy-TT	-5.70/-4.30 eV	TG/BC	150°C	2.04/3.31	Ref. [36]

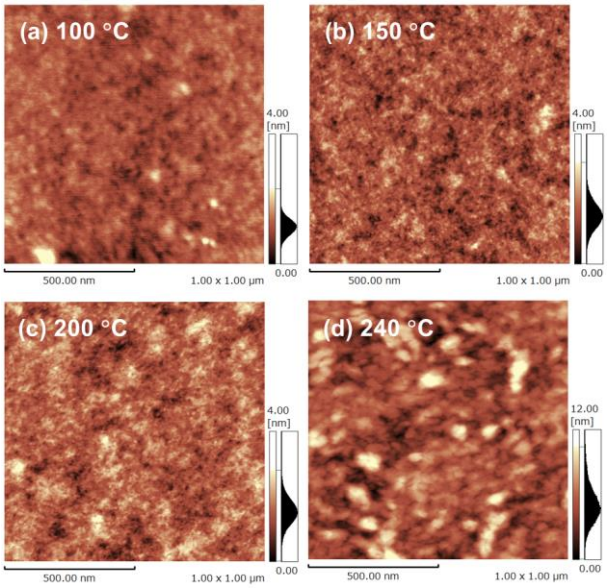

Figure 5. Topographic AFM images of PDPPy-Se films annealed at different temperatures.

As shown in **Figure 5**, the atomic force microscopy (AFM) were obtained for PDPPy-Se thin films annealed at different temperatures. The thin film with T_{anneal} = 100°C showed somewhat aggregation morphology, while larger aggregation of polymers and growth of grains took place with T_{anneal} increment. The RMS (root-mean-square) of the annealed films at 100°C, 150°C and 200°C (before the melting transition temperature) have comparable values of 0.479, 0.521 and 0.572, respectively. The film annealed at 150°C was observed to be more homogeneous with interconnected nanofibrillar networks, which explained the higher mobility. The similar observation was also made for other DPPy-based polymers, and this phenomenon can be linked to the T_{anneal} dependence of OFET performance, *i.e.*, the polymer thin films need to be appropriately

aggregated as excess aggregation induces more grain boundaries detrimental to charge carrier mobility.[25] The RMS of the annealed film at 240°C was significantly increased to 2.029 which indicated a larger-scale crystallite domain resulted from the melting and solidification process since the melting point was determined to be around 240°C from the DSC curve in **Figure 1b**. It has been a commonly acceptable concept that larger crystallite domains result in higher RMS and higher charge carrier mobility. This observation is highly consistent with the device results that both electron and hole mobilities were enhanced for the transistors with the annealing temperature of 240°C compared with the performances of those devices annealed at 100°C, 150°C and 200°C.

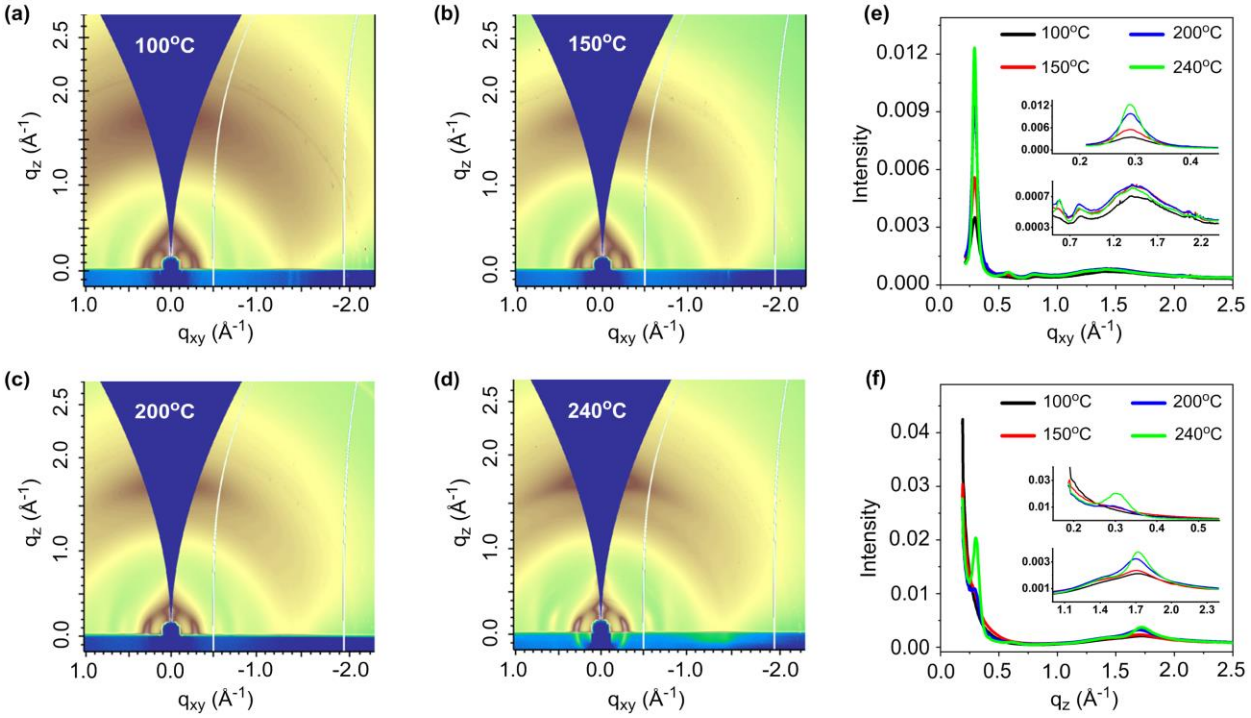

Figure 6. (a-d) 2D-GIWAX patterns of films annealed at 100°C, 150°C, 200°C and 240°C; (e) In-plane (IP) and (f) out-of-plane (OOP) 1D-GIWAXS line cuts (averaged from the 15° pie-slices of the respective 2D-GIWAXS patterns in the horizontal and vertical directions, respectively).

We further employed grazing incidence wide angle X-ray scattering (GIWAXS)[52] to investigate the molecular packing and ordering of the annealed films series. As shown in **Figure 6a-d**, the 2D-GIWAXS patterns exhibit an overall identical morphology with only 1st order alkyl stacking peak near ~ 0.3Å^{-1} (both in and out of plane) and an out of plane π-π stacking peak near ~1.7Å^{-1}. However, detailed analysis of the 1D line profiles in the in and out of plane directions (**Figure 6e-f**) provides evidence that (1) the out-of-plane π-π stacking d-spacing exhibits a fluctuation phenomenon while their coherence length increases monotonically with elevated annealing temperature, and (2) the in-plane lamellar stacking d-spacing remains constant while their coherence length increases monotonically with elevated annealing temperature, see **Table S2** in Supporting Information that summarizes these crystallographic parameters obtained via peak fitting. The raw peak fitting of 1D line cuts of samples annealed at different temperatures is present in **Figure S3** in Supporting Information. Specifically, the 150°C annealed sample displays a closer π-stacking (0.363 nm) compared with the samples annealed at 100°C (0.374 nm) and 200°C (0.367 nm), while their lamellar stacking coherence length increases from 100 nm for 100°C annealed film to 132 nm for 200°C annealed film, explaining, together with its homogeneous surface morphology shown in the AFM images, the overall improvement of crystalline orientation and ordering. Most interestingly, the 240°C annealed sample exhibits not only the closest π-stacking (0.362 nm) but also the largest π-stacking and lamellar stacking coherence length (2.7 nm and 165 nm, respectively) among all the samples. Together, these observations of the 240°C annealed sample clearly point toward the formation of relatively ordered and long-range crystallite domains which correlates well with the significantly increased surface roughness (RMS = 2.029) reported in **Figure 5d**, and thus, delivering the highest OFET performance in both the hole and electron mobilities.

Based on the OFET, AFM and GIWAXS results, we again discuss the carrier mobilities dependent on annealing temperature of 100, 150 and 200°C. It has been reported that DPP-based polymers show reorganization of a microstructure[53] and variation of a grain size and an inter-grain connectivity[25] upon thermal annealing even without any obvious phase transitions, leading to variable OFET performances. Among the three annealing temperatures, 150°C is regarded as the best temperature for reorganizing the polymer microstructure as found in GIWAXS, resulting in the highest carrier mobilities. As the annealing temperature is increased to 200°C, the carrier mobilities are lowered compared to the OFETs annealed at 150°C due to the disturbed π-stacking structures as represented by the farther π-stacking with getting close to the melting point. On the other hand, the lower carrier mobilities of the OFETs annealed at 200°C than those with 100°C annealing is not reasonable based on GIWAXS. Rather, their RMS estimated by AFM implies a slight increase of surface roughness with elevating annealing temperature, which indicates that the low carrier mobilities of the OFETs annealed at 200°C arise from disturbed connectivity between grains.[25] Besides, the significant increase of carrier mobilities with annealing at 240°C can be attributed to the increased crystallinity revealed by GIWAXS and possibly due to subsequent removal of residual water and oxygen molecules acting as carrier traps,[54-55] both of which are mediated by melting. Once again, the significant enhancement of electron transport capability in PDPPy-Se should principally originate from the deepened LUMO level. As for the hole/electron mobility ratio (μ^h/μ^e) dependent on annealing temperature, without melting, μ^h/μ^e ratio is the lowest at 150°C annealing, where μ^e is the best. Thus, it is suggested that PDPPy-Se exhibits electron transport preferable to hole transport when a well-balanced reorganization of polymer backbones and grains takes place. On the other hand, both hole and electron transport capabilities could be

enhanced by improving crystallinity induced by the melting despite the large surface roughness, indicating the crystallinity is a primarily important factor to affect carrier mobilities.

Conclusions

In summary, a pyridine DPP and selenophene based copolymer, PDPPy-Se, was designed and synthesized. The energy levels investigation and comparison with analogous polymers based on other DPP derivatives indicated that both the HOMO and LUMO of PDPPy-Se are lowered. The polymer thin film transistors fabricated from PDPPy-Se delivered an *n*-type-dominant ambipolar property with a maximum electron mobility of 2.22 $cm^2 V^{-1} s^{-1}$ and the hole/electron mobility ratio of 0.0045. The obtained performance is ascribed to the synergistic effects of energy levels and molecular packing and ordering. The lowered HOMO and LUMO can, respectively, increase the hole transfer barrier and decrease the electron transfer barrier. Thus, the hole injection and electron injection from the electrodes into the semiconductors could be suppressed and facilitated, respectively. Additionally, thermal annealing treatment at 240^{o}C promoted the formation of more ordered and longer-range crystallite domains that is favourable for charges transport along the conducting channel in transistors. Specifically, the 240^{o}C annealed film surface was measured to exhibit not only a significantly increased RMS value (from AFM) but also the closest π-π stacking and the largest π-stacking and lamellar stacking coherence length (from GIWAXS experiment) compared with the samples annealed at other temperatures. The synergistic effects of easier electron (compared with hole) injection and favourable charges transport delivered the high-performance *n*-type-dominant performance in OFETs for this copolymer. Overall, in this work, the synergistic use of pyridine and selenophene in the backbone of a diketopyrrolopyrrole-based

copolymer can simultaneously achieve favourable energy levels for electrons injection and tight and ordered molecular packing for charges transport, enhancing the electron mobility and producing *n*-type-dominant ambipolar organic transistors.

Acknowledgments

Q. L. is thankful to QUT for a QUTPRA scholarship to conduct his research. P. S. is thankful to QUT for the financial support from the Australian Research Council (ARC) for the Future Fellowship (FT130101337) and QUT core funding (QUT/322120-0301/07). Work of H.A., I.A. and M. M. N. of NCSU is supported by the General Administration Research Opportunity Initiative grant of University of North Carolina (UNC), and I.A. is also supported by the U.S. Office of Naval Research (ONR, grant No. N000141712204). GIWAXS data was acquired at beamline 7.3.3 in the Advanced Light Source at Lawrence Berkeley National Laboratory (supported by the U. S. Department of Energy, No. DE-AC02-05CH11231); Samuel J. Stuard is acknowledged for his help with X-ray experimental setup and data acquisition at beamline 7.3.3. We thank Dr. Bryan Tuten for the molecular weight determination. Some of the data reported in this paper were obtained at the Central Analytical Research Facility (CARF) operated by the Institute for Future Environments (QUT). Access to CARF is supported by generous funding from the Science and Engineering Faculty (QUT).

References

[1] A. C. Arias, J. D. MacKenzie, I. McCulloch, J. Rivnay, A. Salleo, *Chem. Rev.* **2010**, *110*, 3.

[2] G. Horowitz, *Adv. Mater.* **1990**, *2*, 287.

[3] P. Sonar, H.-S. Tan, S. Sun, Y. M. Lam, A. Dodabalapur, *Polym. Chem.* **2013**, *4*, 1983.

[4] Q. Liu, S. E. Bottle, P. Sonar, *Adv. Mater.* **2020**, *32*, 1903882.

[5] P. Sonar, T. R. Foong, A. Dodabalapur, *Phys. Chem. Chem. Phys.* **2014**, *16*, 4275.

[6] Q. Liu, Y. Wang, A. Kohara, H. Matsumoto, S. Manzhos, K. Feron, S. E. Bottle, J. Bell, T. Michinobu, P. Sonar, *Adv. Funct. Mater.* **2020**, *30*, 1907452.

[7] H. Yin, C. Yan, H. Hu, J. K. W. Ho, X. Zhan, G. Li, S. K. So, *Mat. Sci. Eng. R* **2020**, *140*, 100542.

[8] J. Soyeon, C. Sun, Y. S. Hoon, K. Soon-Ki, C. D. Sung, J. Y. Jin, K. Yun-Hi, *ACS Appl. Mater. Interfaces* **2020**, *12*, 2743.

[9] S. Nikzad, H.-C. Wu, J. Kim, C. M. Mahoney, J. R. Matthews, W. Niu, Y. Li, H. Wang, W.-C. Chen, M. F. Toney, M. He, Z. Bao, *Chem. Mater.* **2020**, *32*, 897.

[10] Z. Chen, M. Li, M. Hu, S. Wang, Z. Miao, S. Xu, C. Chen, H. Dong, W. Huang, R. Chen, *J. Mater. Chem. C* **2020**, *8*, 2094.

[11] C. Zhao, Y. Guo, Y. Zhang, N. Yan, S. You, W. Li, *J. Mater. Chem. A* **2019**, *7*, 10174.

[12] Y. Zhang, L. Tang, H. Sun, S. Ling, K. Yang, M. A. Uddin, H. Guo, Y. Tang, Y. Wang, K. Feng, Y. Shi, J. Liu, S. Zhang, H. Y. Woo, X. Guo, *Macromol. Rapid Commun.* **2019**, *40*, 1900394.

[13] W. Zhang, X. Sun, T. Huang, X. Pan, P. Sun, J. Li, H. Zhang, X. Lu, Q. Fan, W. Huang, *Chem. Commun.* **2019**, *55*, 9487.

[14] H. Zhang, M. Liu, W. Yang, L. Judin, T. I. Hukka, A. Priimagi, Z. Deng, P. Vivo, *Adv. Mater. Interfaces* **2019**, *6*, 1901036.

[15] P. Yuvraj, M. Rajneesh, *Chem. Rec.* **2019**, *19*, 1.

[16] S. Ying, D. Yunfeng, D. Tian, S. Yibo, G. Yanhou, *Mater. Chem. Front.* **2019**, *3*, 1932.

[17] X. Yan, M. Xiong, J. T. Li, S. Zhang, Z. Ahmad, Y. Lu, Z. Y. Wang, Z. F. Yao, J. Y. Wang, X. Gu, T. Lei, *J. Am. Chem. Soc.* **2019**, *141*, 20215.

[18] M. Mone, S. Tang, P. Murto, B. A. Abdulahi, C. Larsen, J. Wang, W. Mammo, L. Edman, E. Wang, *Chem. Mater.* **2019**, *31*, 9721.

[19] Z. a. Li, C.-C. Chueh, A. K. Y. Jen, *Prog. Polym. Sci.* **2019**, *99*, 101175.

[20] M. H. Chua, Q. Zhu, T. Tang, K. W. Shah, J. Xu, *Sol. Energy Mater. Sol. Cells* **2019**, *197*, 32.

[21] J. Y. Back, H. Yu, I. Song, I. Kang, H. Ahn, T. J. Shin, S.-K. Kwon, J. H. Oh, Y.-H. Kim, *Chem. Mater.* **2015**, *27*, 1732.

[22] A. Zhang, C. Xiao, Y. Wu, C. Li, Y. Ji, L. Li, W. Hu, Z. Wang, W. Ma, W. Li, *Macromolecules* **2016**, *49*, 6431.

[23] J. Yao, C. Yu, Z. Liu, H. Luo, Y. Yang, G. Zhang, D. Zhang, *J. Am. Chem. Soc.* **2016**, *138*, 173.

[24] H. Luo, C. Yu, Z. Liu, G. Zhang, H. Geng, Y. Yi, K. Broch, Y. Hu, A. Sadhanala, L. Jiang, P. Qi, Z. Cai, H. Sirringhaus, D. Zhang, *Sci. Adv.* **2016**, *2*, e1600076.

[25] B. Sun, W. Hong, Z. Yan, H. Aziz, Y. Li, *Adv. Mater.* **2014**, *26*, 2636.

[26] Y. Gao, X. Zhang, H. Tian, J. Zhang, D. Yan, Y. Geng, F. Wang, *Adv. Mater.* **2015**, *27*, 6753.

[27] Z. Chen, D. Gao, J. Huang, Z. Mao, W. Zhang, G. Yu, *ACS Appl. Mater. Interfaces* **2016**, *8*, 34725.

[28] K. Broch, D. Venkateshvaran, V. Lemaur, Y. Olivier, D. Beljonne, M. Zelazny, I. Nasrallah, D. J. Harkin, M. Statz, R. D. Pietro, A. J. Kronemeijer, H. Sirringhaus, *Adv. Electron. Mater.* **2017**, *3*, 1700225.

[29] J. Yang, H. Wang, J. Chen, J. Huang, Y. Jiang, J. Zhang, L. Shi, Y. Sun, Z. Wei, G. Yu, Y. Guo, S. Wang, Y. Liu, *Adv. Mater.* **2017**, *29*, 1606162.

[30] H. Yu, H. N. Kim, I. Song, Y. H. Ha, H. Ahn, J. H. Oh, Y.-H. Kim, *J. Mater. Chem. C* **2017**, *5*, 3616.

[31] Q. Liu, H. Sun, C. Blaikie, C. Caporale, S. Manzhos, K. Feron, J. M. MacLeod, M. Massi, S. E. Bottle, J. Bell, Y.-Y. Noh, P. Sonar, *New J. Chem.* **2018**, *42*, 12374.

[32] Q. Liu, H. Sun, S. P. Ponnappa, K. Feron, S. Manzhos, M. W. M. Jones, S. E. Bottle, J. Bell, Y.-Y. Noh, P. Sonar, *Org. Electron.* **2019**, *74*, 290.

[33] Y. Wang, T. Hasegawa, H. Matsumoto, T. Michinobu, *J. Am. Chem. Soc.* **2019**, *141*, 3566.

[34] Z. Wang, Z. Liu, L. Ning, M. Xiao, Y. Yi, Z. Cai, A. Sadhanala, G. Zhang, W. Chen, H. Sirringhaus, D. Zhang, *Chem. Mater.* **2018**, *30*, 3090.

[35] K. Guo, J. Bai, Y. Jiang, Z. Wang, Y. Sui, Y. Deng, Y. Han, H. Tian, Y. Geng, *Adv. Funct. Mater.* **2018**, *28*, 1801097.

[36] B. Sun, W. Hong, H. Aziz, Y. Li, *Polym. Chem.* **2015**, *6*, 938.

[37] C. Y. Yang, W. L. Jin, J. Wang, Y. F. Ding, S. Nong, K. Shi, Y. Lu, Y. Z. Dai, F. D. Zhuang, T. Lei, C. A. Di, D. Zhu, J. Y. Wang, J. Pei, *Adv. Mater.* **2018**, *30*, 1802850.

[38] M. Shahid, T. McCarthy-Ward, J. Labram, S. Rossbauer, E. B. Domingo, S. E. Watkins, N. Stingelin, T. D. Anthopoulos, M. Heeney, *Chem. Sci.* **2012**, *3*, 181.

[39] C.-E. Tsai, R.-H. Yu, F.-J. Lin, Y.-Y. Lai, J.-Y. Hsu, S.-W. Cheng, C.-S. Hsu, Y.-J. Cheng, *Chem. Mater.* **2016**, *28*, 5121.

[40] R. S. Ashraf, I. Meager, M. Nikolka, M. Kirkus, M. Planells, B. C. Schroeder, S. Holliday, M. Hurhangee, C. B. Nielsen, H. Sirringhaus, I. McCulloch, *J. Am. Chem. Soc.* **2015**, *137*, 1314.

[41] K. A. Mazzio, M. Yuan, K. Okamoto, C. K. Luscombe, *ACS Appl. Mater. Interfaces* **2011**, *3*, 271.

[42] I. Kang, T. K. An, J. A. Hong, H. J. Yun, R. Kim, D. S. Chung, C. E. Park, Y. H. Kim, S. K. Kwon, *Adv. Mater.* **2013**, *25*, 524.

[43] J. W. Jung, F. Liu, T. P. Russell, W. H. Jo, *Chem. Commun.* **2013**, *49*, 8495.

[44] I. Osaka, M. Shimawaki, H. Mori, I. Doi, E. Miyazaki, T. Koganezawa, K. Takimiya, *J. Am. Chem. Soc.* **2012**, *134*, 3498.

[45] J.-S. Wu, C.-T. Lin, C.-L. Wang, Y.-J. Cheng, C.-S. Hsu, *Chem. Mater.* **2012**, *24*, 2391.

[46] M. Kim, W.-T. Park, S. U. Ryu, S. Y. Son, J. Lee, T. J. Shin, Y.-Y. Noh, T. Park, *Chem. Mater.* **2019**, *31*, 4864.

[47] G. Oklem, X. Song, L. Toppare, D. Baran, G. Gunbas, *J. Mater. Chem. C* **2018**, *6*, 2957.

[48] J. Lee, A. R. Han, J. Kim, Y. Kim, J. H. Oh, C. Yang, *J. Am. Chem. Soc.* **2012**, *134*, 20713.

[49] Y. Yamaguchi, K. Ogawa, K.-i. Nakayama, Y. Ohba, H. Katagiri, *J. Am. Chem. Soc.* **2013**, *135*, 19095.

[50] Q. Liu, A. Surendran, K. Feron, S. Manzhos, X. Jiao, C. R. McNeill, S. E. Bottle, J. Bell, W. L. Leong, P. Sonar, *New J. Chem.* **2018**, *42*, 4017.

[51] M. Nikolka, G. Schweicher, J. Armitage, I. Nasrallah, C. Jellett, Z. Guo, M. Hurhangee, A. Sadhanala, I. McCulloch, C. B. Nielsen, *Adv. Mater.* **2018**, *30*, 1801874.

[52] A. Hexemer, W. Bras, J. Glossinger, E. Schaible, E. Gann, R. Kirian, A. MacDowell, M. Church, B. Rude, H. Padmore, presented at J. Phys.: Conf. Ser. **2010**.

[53] Z. Chen, M. J. Lee, R. Shahid Ashraf, Y. Gu, S. Albert-Seifried, M. Meedom Nielsen, B. Schroeder, T. D. Anthopoulos, M. Heeney, I. McCulloch, H. Sirringhaus, *Adv. Mater.* **2012**, *24*, 647.

[54] D. F. Figer, *Nature* **2005**, *434*, 192.

[55] R. S. Ashraf, A. J. Kronemeijer, D. I. James, H. Sirringhaus, I. McCulloch, *Chem. Commun.* **2012**, *48*, 3939.

Click here to access/download
Supporting Information
PDPPy-Se_Supporting_12 March 2020.docx

Click here to access/download
Production Data
PDPPy-Se_Manuscript_12 March 2020_Without Highlight.pdf

Click here to access/download
Production Data
PDPPy-Se_Supporting_12 March 2020_Without Highlight.pdf

Click here to access/download
Production Data
Response Letter_ Advanced Functional Materials.pdf